ORIGINAL ARTICLE

Astronomische Nachrichten

Bright spectroscopic binaries: II. A study of five systems with orbital periods of $P \lesssim 500$ days

Dennis Jack[1] | **Missael Alejandro Hernández Huerta**[1] | **Faiber Danilo Rosas-Portilla**[1] | **Klaus-Peter Schröder**[1,2]

[1]Departamento de Astronomía, Universidad de Guanajuato, Guanajuato, Mexico

[2]Sterrewacht Leiden, Universiteit Leiden, Leiden, Netherlands

Correspondence
Dennis Jack, Departamento de Astronomía, Universidad de Guanajuato, Callejón de Jalisco S/N, 36023 Guanajuato, GTO, Mexico.
Email: dennis.jack@ugto.mx

Funding information
CONACyT-DFG, Grant/Award Number: 278156; Universidad de Guanajuato, Grant/Award Numbers: 036/2021, 105/2021

Abstract

We present a detailed analysis of five bright spectroscopic binary systems (HD 18665, HD 27131, HD 171852, HD 215550, and HD 217427) that have orbital periods of $P \lesssim 500$ days. We determined the complete set of orbital parameters using the toolkit RadVel by analyzing the observed radial velocity curves. To study the properties of the five systems, we also analyzed the intermediate resolution spectra ($R \approx 20{,}000$) observed with the TIGRE telescope and determined the stellar parameters of the primary stars using the toolkit iSpec. With Gaia Early Data Release 3 parallaxes, a correction for interstellar extinction using the 3D dust map, and bolometric corrections, we placed the stars in the Hertzsprung-Russell diagram and compared the positions with stellar evolution tracks calculated with the Eggleton code to determine the masses and ages of the primary stars. They have all evolved to the giant phase. Finally, we were able to determine the masses of the secondary stars and to estimate the orbital inclinations i of the binary systems.

KEYWORDS

binaries: spectroscopic, HD 171852, HD 215550, HD 217427, HD 27131, stars: fundamental parameters, stars: individual (HD 18665), techniques: radial velocities

1 | INTRODUCTION

Multiple stellar systems are a natural outcome of the star formation process (Duchêne & Kraus 2013; Tohline 2002), and a binary fraction of 50% in the solar neighborhood has been estimated by Raghavan et al. (2010). Fisher et al. (2005) showed that well-separated binaries like in this paper form a large fraction of the stellar galactic content. Binary or multiple stars are important objects, because they offer the opportunity to determine the masses of the components directly. This is impossible for single stellar objects. The stellar mass is an important parameter for the understanding of the evolution of stars.

There exist several detection methods for binary systems. One important method is the detection of periodic variations in the radial velocity (RV) by spectroscopic analysis of the stars. In fact, the first exoplanet orbiting a main-sequence star was also discovered with this method (Mayor & Queloz 1995). Detecting and studying spectroscopic binary systems requires an intermediate to high spectral resolution, but the signal-to-noise ratio (S/N) can still be relatively low. A wide spectral range is also helpful for a more precise determination of the RV using a large number of spectral lines. Several observations at different epochs are necessary to detect the RV changes and to confirm the binarity of the star system. Usually, only the

primary star is visible in the spectrum (SB1), but if the two stars have similar luminosities, spectral lines of the secondary star will appear in the observed spectrum (SB2). It is possible to determine the orbital parameters using many observations at different epochs obtaining a well covered RV curve. This allows conclusions about the invisible secondary star in case of an SB1 system, which are the objects we were studying in this publication.

In our first publication of this series (Jack et al. 2020) (hereafter Paper I), we presented details of our observation campaign with the Telescopio Internacional de Guanajuato Robótico Espectroscópico (TIGRE) telescope and reported the discovery of 19 bright binary star systems ($m_V < 7.66$ mag). Because they have very different orbital periods, we presented a detailed analysis of only five binary systems with short orbital periods of less than 1 year in Paper I. In the present publication, we show the results of further five bright binary systems with orbital periods of $P \lesssim 500$ days. The remaining bright binary stars have even longer periods, and we will continue with our observation campaign to determine their orbital parameters and will present the results in following publications.

For this work, we improved several aspects of our methods for the analysis of the RV curves and the determination of stellar parameters. One important improvement is the use of the recently published Gaia EDR3 catalog (Gaia Collaboration et al. 2020; Lindegren, Klioner, et al. 2020a; Lindegren, Bastian, et al. 2020b) of the European Space Agency (ESA) Gaia mission (Gaia Collaboration et al. 2016), because it contains improved parallaxes for our stars. To obtain more precise luminosities, we now correct the effects of interstellar extinction using the 3D dust mapping. Furthermore, we improved our method for the determination of the stellar parameters, like effective temperature and surface gravity.

2 | BINARY ORBITS

2.1 | RV curves

The stars were observed with the 1.2 m robotic telescope TIGRE (Schmitt et al. 2014) situated near Guanajuato,

Central Mexico. It is equipped with the HEROS spectrograph with an intermediate resolution of $R \approx 20{,}000$. We obtained a time series of optical spectra in the wavelength range from about 3,800 to 8,800 Å, with a small gap of about 120 Å around 5,800 Å. The exposure time of each spectrum was 1 min. The RVs were determined with the procedure described in Paper I and in Mittag et al. (2018). All individual RV measurements can be found in Table A1 and are also electronically available as Data S1–S6.

Note that HD 27131 has already been identified as a spectroscopic binary by Houk & Swift (1999). They state that the spectrum is a composition of a K0 giant and an A3 star. We confirm that HD 27131 is in fact an SB2 star. However, no further observations, detailed RV measurements, or orbital parameters had been reported, so far.

2.2 | Orbital parameters

We used the RV Modeling Toolkit RadVel (Fulton et al. 2018) (version 1.4.6) to analyze the RV curves and to determine the orbital parameters of the binaries. These parameters were the orbital period P, the time of inferior conjunction T_c, eccentricity e, semi-amplitude K, the argument of the periapsis of the star's orbit ω, and the RV of the system v_{rad}. After inserting initial guesses for the six orbital parameters, the set of equations for the Keplerian orbit was solved by an iterative method to determine the best fit for the observed RV curve. To obtain an estimation of the uncertainties, we used the Markov-Chain Monte Carlo (MCMC) package of Foreman-Mackey et al. (2013) included in RadVel.

In Table 1, we present the results of the RadVel run, including the errors that we obtained with the MCMC run. One star has an orbital period of less than 1 year, but was not presented in Paper I. The orbits of the stars have a notable eccentricity e that allowed a determination of their argument of the periapsis ω. The semi-amplitudes K of the orbits range from 8 to almost 21 km s^{-1}.

In Figure 1, we plotted the observed RV curve and the RadVel fit of HD 18665. The star HD 27131 has the largest semi-amplitude ($K = 20.96$ km s^{-1}) of all five stars and a

TABLE 1 The orbital parameters of five spectroscopic binary systems determined with RadVel

Star	P (days)	T_c (JD)	e	K (km s^{-1})	ω (rad)	v_{rad} (km s^{-1})
HD 18665	506.0 ± 1.5	$8{,}308.5 \pm 3.3$	0.482 ± 0.013	8.00 ± 0.14	5.611 ± 0.029	-5.052 ± 0.072
HD 27131	464.1 ± 1.6	$8{,}229.9 \pm 3.2$	0.1215 ± 0.0092	20.96 ± 0.24	5.315 ± 0.077	22.43 ± 0.21
HD 171852	348.58 ± 0.16	$8{,}275.93 \pm 0.57$	0.2651 ± 0.0032	14.231 ± 0.058	4.89 ± 0.01	-27.515 ± 0.034
HD 215550	436.76 ± 0.24	$8{,}716.86 \pm 0.23$	0.3619 ± 0.0023	18.243 ± 0.045	1.5307 ± 0.0081	-0.182 ± 0.036
HD 217427	416.5 ± 1.2	$8{,}369.7 \pm 3.3$	0.415 ± 0.013	9.13 ± 0.17	4.501 ± 0.024	-25.01 ± 0.08

FIGURE 1 Radial velocity (RV) curve of HD 18655: (a) the complete measurements (circles) and RadVel fit (solid line), (b) the residuals, and (c) the phase-folded RV curve
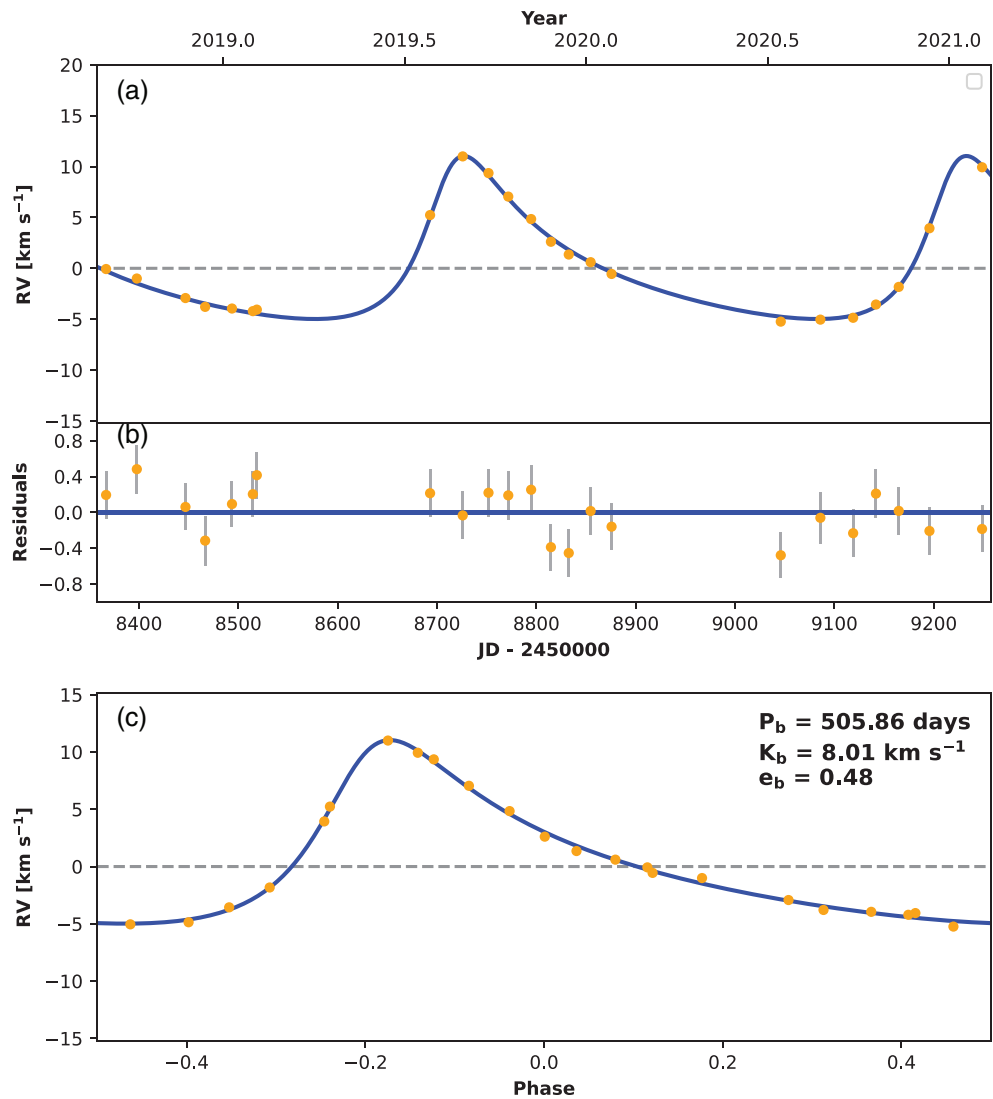
low eccentricity as can be seen in the RV curve in Figure 2. In Figure 3, we present the complete RV measurements of the star HD 171852. The orbital period is very close to 1 year, and the RV measurements cover more than two orbits. Figure 4 demonstrates the RV curve of HD 215550. The last star of our sample is HD 217427 and the RV curve is shown in Figure 5. The lower part of the RV curve is not well covered.

HD 217427 has an entry in the wide binary catalog of Tian et al. (2020) with an angular separation of about 144 arcseconds to its companion star. This orbit is at a very far distance from the secondary orbit found in this work, so that this system is probably a hierarchical triple star system.

3 | STELLAR PARAMETERS

We determined all stellar parameters of the primary stars by analyzing the intermediate resolution spectra ($R \approx$

20,000) obtained with the TIGRE telescope. By locating the stars in the Hertzsprung-Russell diagram (HRD) and comparing the positions with stellar evolution tracks, we were also able to determine the masses and ages of the systems.

3.1 | Distances, extinction, and absolute magnitudes in V

We list the observational properties like spectral type and apparent magnitude in the V-band (m_V) as given in the SIMBAD database in Table 2. The parallaxes in milliarcseconds (and distances in parsecs) were taken from the Gaia EDR3 archive, and we applied the parallax zero-point correction (Lindegren et al. 2020b) using the published Python code. There exist a possibly large systematic effect on the Gaia EDR3 parallaxes because of the binarity of the objects as was already discussed in Paper I. All stars are giants (small M_V), and some are located at distances, where reddening will affect the observed photometry.
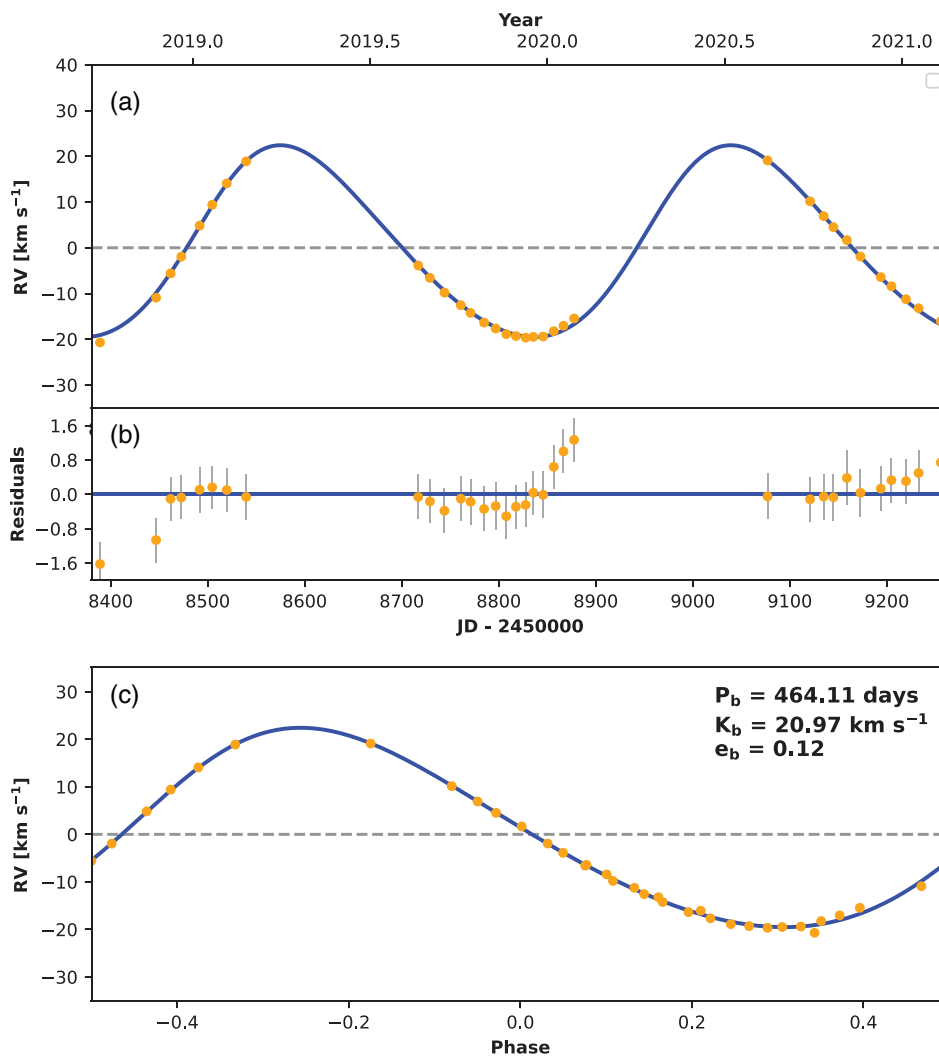
FIGURE 2 Radial velocity (RV) curve of HD 27131: (a) the complete measurements (circles) and RadVel fit (solid line), (b) the residuals, and (c) the phase-folded RV curve

We estimated the reddening using the 3D dust mapping (Green et al. 2019) (http://argonaut.skymaps.info/) and obtained the color excess $E(B-V)$ using the dust map at the given positions and Gaia EDR3 distances. We assumed an extinction law of $R(V) = 3.1$ to obtain the correction for the V-band (A_V) magnitude. The Gaia EDR3 distances with the correction of extinction were then used to determine the absolute magnitudes in the V-band (M_V). To determine the bolometric magnitudes and luminosities, it was necessary to apply bolometric corrections (BC), for which exact stellar parameters, especially the effective temperature T_{eff}, were required. Thus, a detailed analysis of the observed spectra was necessary before we could estimate the BCs and calculate the luminosities of the five stars.

3.2 | Spectral analysis

We obtained intermediate resolution spectra with an S/N that was sufficient to determine the individual RVs. The

mean S/N of a spectrum in the red channel was about 30, while in the blue channel, depending on the spectral type, the S/N had values between 5 and 10. To obtain one spectrum with a high S/N, we combined ten spectra with the highest S/N. Before, each individual spectrum was corrected for the RV.

For the determination of the stellar parameters, we used the spectral analysis toolkit iSpec (Blanco-Cuaresma et al. 2014) in its Python 3 version (v2020.10.01) (Blanco-Cuaresma 2019). It allowed us to compare observed spectra with synthetic spectra determining the selected free parameters by a χ^2 method.

We used the grid of Model Atmospheres in Radiative and Convective Scheme (MARCS) atmosphere models (Gustafsson et al. 2008) included in iSpec. For the reference solar abundances, we used the values published in Grevesse et al. (2007). The synthetic spectra were calculated using the radiative transfer code *turbospectrum* (Alvarez & Plez 1998; Plez 2012), because it used spherical symmetry, which is more accurate for giant stars. The list of atomic lines was taken from the Vienna Atomic

FIGURE 3 Radial velocity (RV) curve of HD 171852: (a) the complete measurements (circles) and RadVel fit (solid line), (b) the residuals, and (c) the phase-folded RV curve
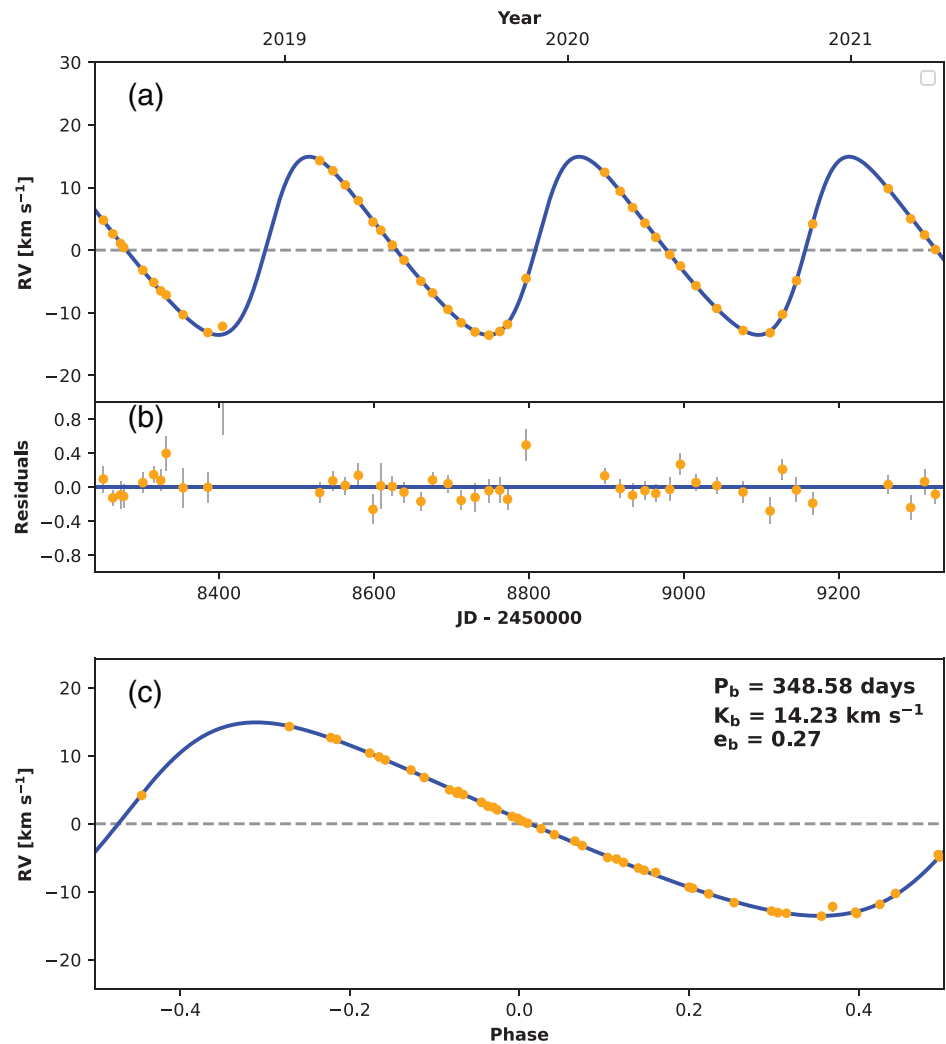

Line Data Base (VALD) (Kupka et al. 2011; Piskunov et al. 1995).

We have developed different methods for the determination of stellar parameters with iSpec. One method was used in a previous work with exoplanet hosting main sequence stars (Flor-Torres et al. 2021), and a different method was developed as an attempt to quickly determine stellar parameters (Schröder et al. 2021). In this work, we applied the improved method established in Rosas Portilla et al. (2021) that works very well with giant stars.

Because we did not have any known initial values (no SIMBAD entries), we used an estimation of the initial values with a comparison to precalculated grid spectra. In the first step, the improved method found the best continuum fit using individually determined continuum regions for each spectrum based on a precalculated synthetic spectrum using the estimated initial values. The method then used a defined set of spectral lines for the comparison between observed and theoretical spectra. In that way, it determined the complete set of stellar parameters, which were the effective temperature T_{eff}, surface gravity $\log g$,

metallicity [M/H], alpha enhancement [α/Fe], the micro turbulence v_{mic}, macro turbulence v_{mac}, and rotational velocities $v_{\text{rot}} \sin i$. We then varied the initial values for T_{eff}, $\log g$, and [M/H] and calculated a total of 27 possible fits. The final fit was the one with the lowest root mean square. Further details of the method and thorough tests were presented in Rosas Portilla et al. (2021).

We present the final stellar parameters in Table 3. The effective temperatures range from about 4200 to 5100 K. The surface gravities are consistent with the fact that all stars are giants. HD 27131 has a low metallicity of [M/H] = −0.31. It is worth to state that the determination of the rotational velocity ($v_{\text{rot}} \sin i$) has improved with the new method. Some rotational velocities in Paper I was too large. The rotational velocities represent now expected values for giant stars, but it was not possible to determine rotational and also macro turbulence velocities that have values of less than 3 km s^{-1} because of the intermediate resolution and the resulting instrumental profile of the HEROS spectrograph (Schröder et al. 2021). For HD 27131, we found that $v_{\text{rot}} \sin i$ = 6.3 km s^{-1}. The rotational
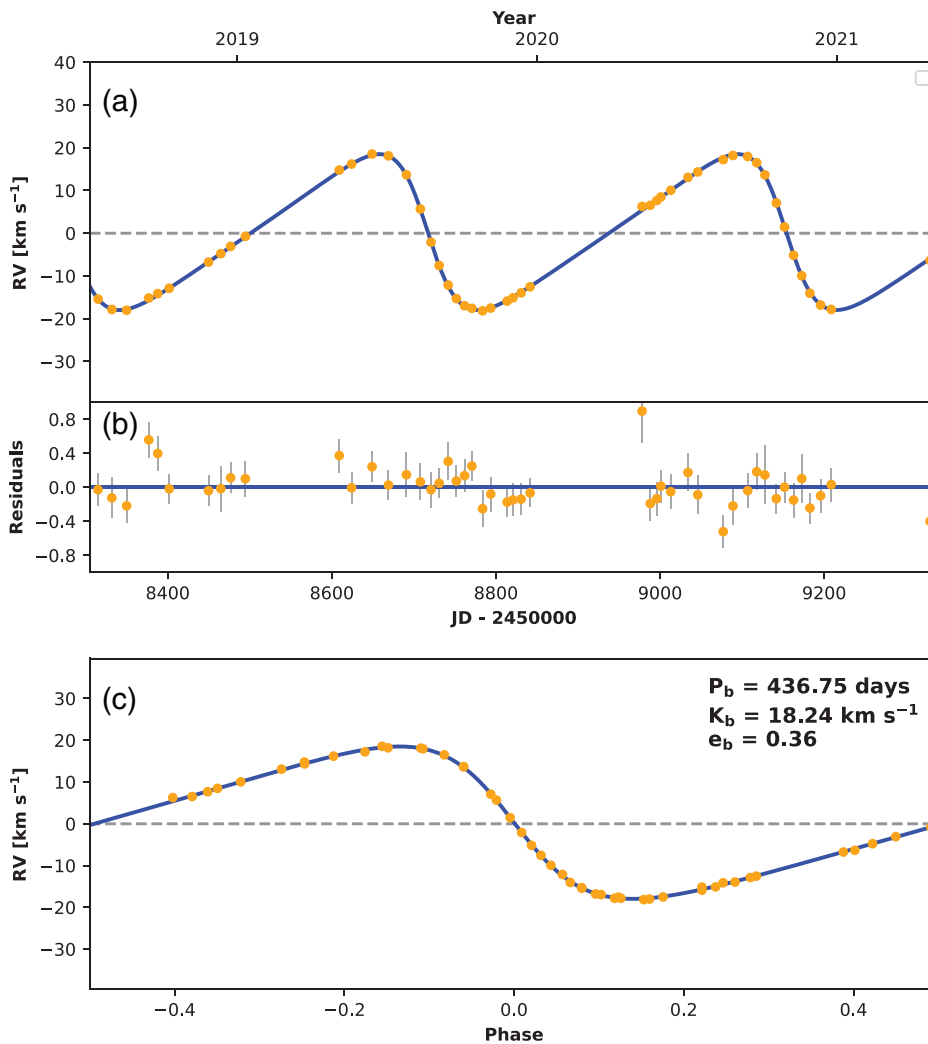
FIGURE 4 Radial velocity (RV) curve of HD 215550: (a) the complete measurements (circles) and RadVel fit (solid line), (b) the residuals, and (c) the phase-folded RV curve

velocities include a factor of $\sin i$ because of the inclination of the stellar rotation axis, which is likely to be close to $i = 90°$, because we observed spectroscopic binaries. Of course, we assumed that the inclination of the rotation axis of the primary stars and of the orbits around the companion stars are similar. Below, we will give an estimate of the orbital inclination i of the binary system orbits.

3.3 | Masses and ages

Using the BCs calculated with the published code presented in Casagrande & VandenBerg (2014, 2018), we obtained the absolute bolometric magnitudes M_{bol} of the stars. The script determined the BCs based on the three stellar parameters T_{eff}, $\log g$, and [M/H]. We calculated the luminosity L (in solar luminosities $L_\odot$) and present the results in Table 4. Having the luminosities and effective temperatures (Table 3) of the primary stars, we could place them in the HRD. We used stellar evolution tracks that we computed with the Cambridge (UK) Eggleton code

in its updated version (Pols et al. 1997; Pols et al. 1998). The Eggleton code overshooting parameter, and in consequence, the blue loop luminosity for any given intermediate mass, has been accurately tested with giants of zeta Aurigae systems of well known mass and luminosity (Schroder et al. 1997). The results are presented in Table 4. The masses ranged from 1.9 to 3.4 $M_\odot$, and the ages from 280 Myr to $\approx$ 1.4 Gyr. The errors of the ages are relatively large because the evolution tracks are very close together during the giant phase. In Figure 6, we show the positions of HD 18665 and HD 27131 in the theoretical HRD with $Z = 0.01$ stellar evolution tracks. The HRD positions of the other three stars (HD 171852, HD 215550, HD 217427) are presented in Figure 7, where the evolution tracks were calculated assuming solar metallicity ($Z = 0.02$). Not all stars were classified as giant stars in SIMBAD. Please note that the errors in Table 4 are so small thanks to the stars being on the L-sensitive part of their blue loops.

As a consistency check, we calculated the parallax-related surface gravities of all stars as described in Rosas Portilla et al. (2021). Knowing the luminosity L,
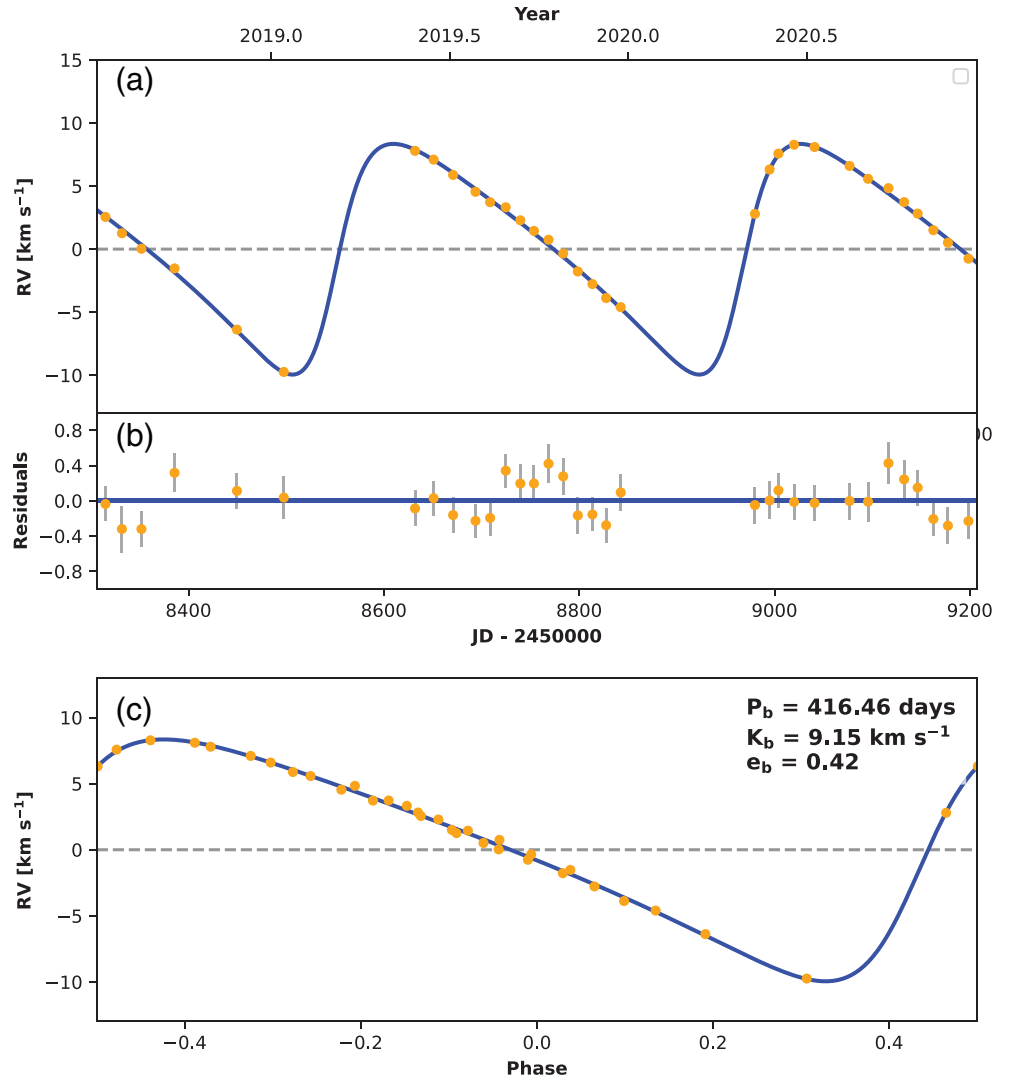
FIGURE 5 Radial velocity (RV) curve of HD 217427: (a) the complete measurements (circles) and RadVel fit (solid line), (b) the residuals, and (c) the phase-folded RV curve

TABLE 2 Observational properties of five spectroscopic binary stars

| Star	Spectral type	m_V	Parallax (mas)	Distance (pc)	$E(B-V)$	M_V
HD 18665	K2	7.25 ± 0.01	2.713 ± 0.126	373.5 ± 13.1	0.118 ± 0.02	-0.98 ± 0.1
HD 27131	K0III+A3	6.94 ± 0.01	4.402 ± 0.047	228.9 ± 0.8	0.22 ± 0.03	-0.54 ± 0.09
HD 171852	G8III/IV	6.61 ± 0.01	10.897 ± 0.085	92.1 ± 0.4	0.0 ± 0.01	1.79 ± 0.03
HD 215550	G5	7.20 ± 0.01	3.078 ± 0.093	328.8 ± 6.2	0.065 ± 0.02	-0.59 ± 0.08
HD 217427	K2	6.70 ± 0.01	3.764 ± 0.094	268.2 ± 4.2	0.125 ± 0.02	-0.83 ± 0.07

Note: The extinction ($E(B-V)$) was determined with the 3D dust map in order to obtain the absolute magnitudes M_V.

**TABLE 3** Basic stellar parameters of the five spectroscopic binaries determined with spectral analysis using iSpec

Star	T_{eff} (K)	$\log g$	$[M/H]$	$[\alpha/Fe]$	v_{mic} (km s^{-1})	v_{mac} (km s^{-1})	$v_{\text{rot}} \sin i$ (km s^{-1})
HD 18665	$4,253 \pm 23$	1.81 ± 0.04	-0.15 ± 0.02	0.03 ± 0.03	1.93 ± 0.03	4.19 ± 0.54	0.45 ± 1.63
HD 27131	$5,047 \pm 69$	2.63 ± 0.14	-0.31 ± 0.06	-0.05 ± 0.06	0.80 ± 0.06	2.40 ± 2.80	6.31 ± 0.84
HD 171852	$5,096 \pm 40$	3.17 ± 0.10	-0.01 ± 0.03	-0.03 ± 0.04	1.36 ± 0.05	3.07 ± 0.82	0.00 ± 0.00
HD 215550	$5,063 \pm 47$	2.76 ± 0.12	0.02 ± 0.04	-0.03 ± 0.05	1.33 ± 0.05	3.15 ± 0.84	0.00 ± 0.00
HD 217427	$4,603 \pm 19$	2.49 ± 0.05	0.08 ± 0.02	-0.06 ± 0.03	1.38 ± 0.03	0.00 ± 0.74	0.00 ± 0.00

TABLE 4 The masses and ages of the five primary stars of the spectroscopic binaries determined with fitting stellar evolution tracks to the positions in the HRD

Star	M_V	BC	M_{bol}	$\log T_{eff}$	$\log L/L_\odot$	Mass ($M_\odot$)	Age (Myr)
HD 18665	-0.98 ± 0.10	-0.59 ± 0.02	-1.56 ± 0.10	3.639 ± 0.002	2.55 ± 0.04	1.90 ± 0.05	1357^{+94}_{-98}
HD 27131	-0.54 ± 0.09	-0.23 ± 0.02	-0.77 ± 0.10	3.703 ± 0.006	2.23 ± 0.04	2.96 ± 0.18	401^{+124}_{-84}
HD 171852	1.79 ± 0.03	-0.20 ± 0.02	1.59 ± 0.04	3.707 ± 0.003	1.29 ± 0.02	1.95 ± 0.05	1303^{+104}_{-94}
HD 215550	-0.59 ± 0.08	-0.21 ± 0.02	-0.80 ± 0.08	3.704 ± 0.004	2.24 ± 0.03	3.40 ± 0.05	279^{+12}_{-11}
HD 217427	-0.83 ± 0.07	-0.42 ± 0.02	-1.25 ± 0.07	3.663 ± 0.002	2.42 ± 0.03	3.00 ± 0.20	394^{+199}_{-59}
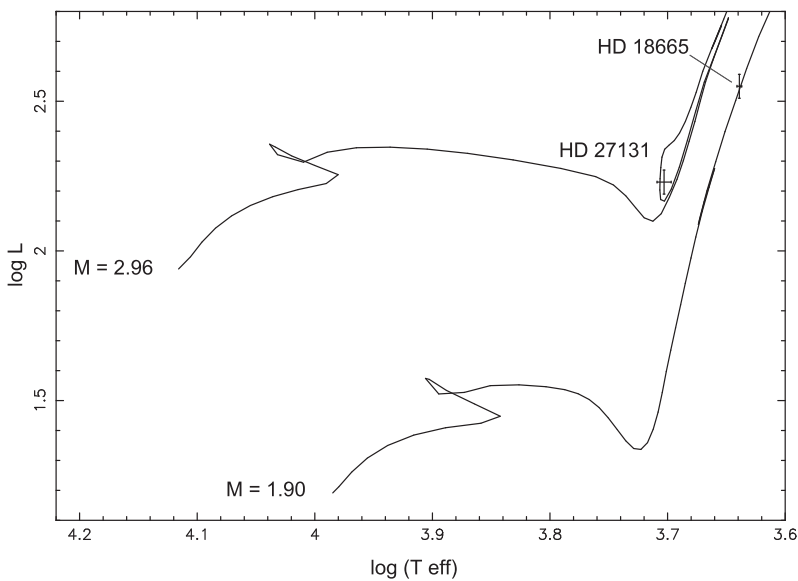
FIGURE 6 Positions of HD 18665 and HD 27131 in the HRD and the best fitting stellar evolution tracks (solid lines) of the respective masses using tracks with $Z = 0.01$. All stars are in the giant phase
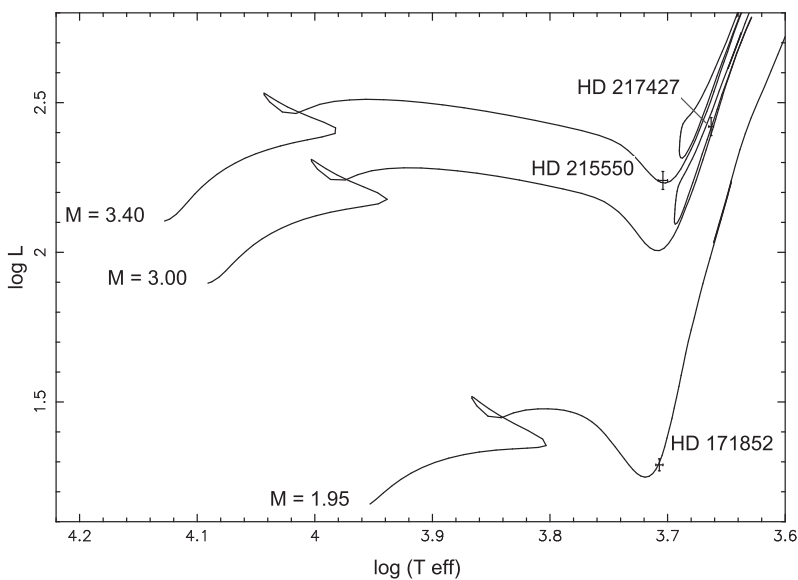
FIGURE 7 Positions of HD 171852, HD 215550, and HD 217427 in the HRD and the best fitting stellar evolution tracks (solid lines) of the respective masses using tracks with solar metallicity ($Z = 0.02$). All stars are in the giant phase

TABLE 5 The mass function (f) of the five spectroscopic binary systems, which we used to determine the minimum mass of the secondary stars (m_2). The inclinations i were determined

Star	f ($M_\odot$)	M_1 ($M_\odot$)	$m_2 = M_2 \sin i$ ($M_\odot$)	$m_2^\dagger \sqrt{r}$ (M_{Jup})	γ	i	M_2 ($M_\odot$)
HD 18665	0.0181 ± 0.0006	1.90 ± 0.05	0.41 ± 0.01	194^{+64}_{-40}	0.204	$45.3°^{+11.8°}_{-6.2°}$	0.58 ± 0.1
HD 27131	0.433 ± 0.015	2.96 ± 0.18	1.72 ± 0.07	83^{+29}_{-19}	0.216	$79.9°^{+2.4°}_{-3.3°}$	1.75 ± 0.07
HD 171852	0.0933 ± 0.0009	1.95 ± 0.05	0.74 ± 0.01	22^{+8}_{-6}	0.043	$69.0°^{+5.9°}_{-6.0°}$	0.79 ± 0.04
HD 215550	0.2226 ± 0.0011	3.40 ± 0.05	1.45 ± 0.02	98^{+32}_{-19}	0.207	$77.0°^{+2.7°}_{-3.8°}$	1.49 ± 0.05
HD 217427	0.0247 ± 0.0010	3.00 ± 0.20	0.61 ± 0.03	12^{+30}_{-19}	0.187	$87.0°^{+3.0°}_{-4.9°}$	0.61 ± 0.03

the mass M_1, and the distance from Gaia EDR3, we calculated the surface gravity using basic relations between the stellar parameters. We found that the two independently determined surface gravities are very similar. The largest difference was found for HD 217427 with $\Delta \log g \approx 0.4$, but this comes probably from the uncertain interstellar extinction $E(B - V)$ of that star.

3.4 | Secondary star masses and orbital inclination i

As explained in more detail in Paper I, one can use the Kepler's laws to derive a formula that connects the masses of the two components of a binary system with three observable orbital parameters, which are the orbital period P, semi-amplitude K, and the eccentricity e. This so called mass function f is calculated by the formula.

$$f = \frac{M_2^3 \sin^3 i}{(M_1 + M_2)^2} = \frac{PK^3}{2\pi G}\left(1 - e^2\right)^{3/2}, \qquad (1)$$

where G represents the gravitational constant. The mass function f allows to calculate both masses from one spectroscopic orbit only, if both inclination i and the mass ratio are known. This is only the case for eclipsing SB2 systems (i.e., $\sin i$ close to 1). Alternatively, $\sin i$ can be obtained from an astrometric orbit, where available. However, in the cases of ordinary SB1 systems, as treated by this paper, the strategy can only be to obtain the masses, and hence the mass ratio, from the photometric parameters and parallax of the system. In turn, the mass function then allows to estimate $\sin i$. Because we determined the masses of the primary stars (M_1), we could calculate the minimal masses of the secondary stars ($m_2 = M_2 \sin i$) solving Equation (1). We present the values for the mass function f and the minimal secondary masses (m_2) in Table 5.

Our five binary stars were also identified as binaries by Kervella et al. (2019) in an analysis of the proper motion anomaly of Hipparcos stars using Gaia DR2 data. They also determined the masses of the secondary stars normalized

for a 1 AU circular orbit $m_2^\dagger$, which was related to the minimal mass of the secondary by the relation $m_2^\dagger \sqrt{r}$, where r was the orbital distance (in AU) from the primary, unknown for them.

We could calculate the minimal masses of Kervella et al. (2019) using the orbital distance r from our orbital parameters using the Kepler's laws. The orbital distance of the primary is given by

$$r = a_1 = \left(\frac{G}{4\pi^2}\frac{M_2^3}{M_{tot}^2}P^2\right)^{1/3}. \qquad (2)$$

We could then calculate the minimal mass of the secondary assuming a circular orbit. The orbit of the binary is projected in the sky, and the variation in the proper motion has its maximum for an inclination of $i = 0°$. This is the complete opposite projection than for the orbit determined with RV measurements, where the maximum effect is found at an inclination of $i = 90°$. The Kervella et al. (2019) minimal masses are related to the actual secondary mass M_2 by $\cos i$, while the minimal masses from the RV curves are related to the actual mass by $\sin i$. Combining these two minimal masses, we determined the orbital inclination i using the equation

$$i = \arctan\frac{m_2}{m_2^\dagger \sqrt{r}}. \qquad (3)$$

In addition, we calculated the actual mass of the secondary with the equation $M_2 = m_2 / \sin i$.

For orbital periods that are smaller or close to the observing window of Gaia DR2 ($\delta t = 668$ days), the observed effect of a proper motion anomaly will decrease because of a smearing effect of the signal. Kervella et al. (2019) demonstrated the impact of this effect in their Figure 2. The graph showed us that binary systems with periods presented in this work are affected by this smearing effect with a factor of roughly $\gamma \approx 0.2$. Because we know the exact period of each binary system, we could calculate the sensitivity factor γ using Equation 13 of Kervella et al. (2019). This factor increased the actual signal and increased their normalized minimal secondary masses $m_2^\dagger$.

The factor γ and the results for the inclination i and the secondary mass M_2 are presented in Table 5. All orbital inclinations i are closer to 90° than to 0°. The lowest inclination has the star HD 18665 ($i = 45.3°$). Because of the large inclinations, the masses of the secondary stars M_2 are very similar to the minimal masses m_2 determined before. Even for HD 18665 ($m_2 = 0.41\ M_\odot$) the secondary mass is still less than solar ($M_2 = 0.58\ M_\odot$).

It is important to mention that the orbital inclinations determined with this method are very sensitive to the values of Kervella et al. (2019). The low sensitivity factor γ increased this even further. Thus, the inclinations presented here may not be very reliable. There is even the possibility that they measured the effect of a different companion star and further member of the system or a combination effect of several stars in a multiple stellar system.

4 | SUMMARY

In the second publication of our series about bright spectroscopic binaries, we determined the stellar and orbital parameters of five binary systems with orbital periods of about $P \lesssim 500$ days. Using intermediate resolution spectra, we determined the stellar parameters of the five stars with an improved method for iSpec. With Gaia EDR3 parallaxes considering interstellar extinction and BCs, we determined the masses and ages by a comparison of the HRD positions with stellar evolution tracks calculated with the Eggleton code. Finally, an estimation of the masses of the respective secondary stars was presented. Using the results of an analysis of proper motions anomaly of Kervella et al. (2019), we estimated the orbital inclinations of the binary systems and could determine the absolute secondary star masses. We found that three of the primary stars were not classified as giants in the SIMBAD database, and no star as spectroscopic binary.

ORCID

Dennis Jack https://orcid.org/0000-0003-3343-6743
Missael Alejandro Hernández Huerta https://orcid.org/0000-0002-1579-4910

REFERENCES

Alvarez, R., & Plez, B. 1998, *A&A*, *330*, 1109.

Blanco-Cuaresma, S. 2019, *MNRAS*, *486*(2), 2075.

Blanco-Cuaresma, S., Soubiran, C., Heiter, U., & Jofré, P. 2014, *A&A*, *569*, A111.

Casagrande, L., & VandenBerg, D. A. 2014, *MNRAS*, *444*(1), 392.

Casagrande, L., & VandenBerg, D. A. 2018, *MNRAS*, *475*(4), 5023.

Duchêne, G., & Kraus, A. 2013, *ARA&A*, *51*(1), 269.

Fisher, J., Schröder, K.-P., & Smith, R. C. 2005, *MNRAS*, *361*(2), 495.

Flor-Torres, L. M., Coziol, R., Schröder, K. P., Jack, D., Schmitt, J. H. M. M., & Blanco-Cuaresma, S. 2021, *Rev. Mexicana Astron. Astrofis.*, *57*, 199.

Foreman-Mackey, D., Hogg, D. W., Lang, D., & Goodman, J. 2013, *PASP*, *125*(925), 306.

Fulton, B. J., Petigura, E. A., Blunt, S., & Sinukoff, E. 2018, Apr, *PASP*, *130*(986), 044504.

Gaia Collaboration, Brown, A. G. A., Vallenari, A., Prusti, T., de Bruijne, J. H. J., et al. 2020, *A&A*, *649*, A1. https://doi.org/10.1051/0004-6361/202039657.

Gaia Collaboration, Prusti, T., de Bruijne, J. H. J., et al. 2016, November, *A&A*, *595*, A1.

Green, G. M., Schlafly, E., Zucker, C., Speagle, J. S., & Finkbeiner, D. 2019, *ApJ*, *887*(1), 93.

Grevesse, N., Asplund, M., & Sauval, A. J. 2007, *Space Sci. Rev.*, *130*(1–4), 105, 114.

Gustafsson, B., Edvardsson, B., Eriksson, K., Jørgensen, U. G., Nordlund, Å., & Plez, B. 2008, *A&A*, *486*(3), 951.

Houk, N., & Swift, C. 1999, *Michigan Spectral Survey*, Vol. *5*. University of Míchigan (Ann Arbor).

Jack, D., Hernández Huerta, M. A., & Schröder, K.-P. 2020, *Astronomische Nachrichten*, *341*, 616.

Kervella, P., Arenou, F., Mignard, F., & Thévenin, F. 2019, *A&A*, *623*, A72.

Kupka, F., Dubernet, M. L., & VAMDC Collaboration 2011, *Baltic Astron.*, *20*, 503.

Lindegren, L., Klioner, S. A., Hernández, J., et al. 2020a, *A&A*, *649*, A2. https://doi.org/10.1051/0004-6361/202039709.

Lindegren, L., Bastian, U., Biermann, M., et al. 2020b, *A&A*, *649*, A4. https://doi.org/10.1051/0004-6361/202039587.

Mayor, M., & Queloz, D. 1995, *Nature*, *378*(6555), 355.

Mittag, M., Hempelmann, A., Fuhrmeister, B., Czesla, S., & Schmitt, J. H. M. M. 2018, *AN*, *339*, 53.

Ochsenbein, F., Bauer, P., & Marcout, J. 2000, *Astron. Astrophys. Suppl. Ser.*, *143*, 23.

Piskunov, N. E., Kupka, F., Ryabchikova, T. A., Weiss, W. W., & Jeffery, C. S. 1995, *A&AS*, *112*, 525.

Plez, B. (2012), *Turbospectrum: Code for Spectral Synthesis*. Astrophysics Source Code Library (Montpellier).

Pols, O. R., Schröder, K.-P., Hurley, J. R., Tout, C. A., & Eggleton, P. P. 1998, *MNRAS*, *298*(2), 525.

Pols, O. R., Tout, C. A., Schroder, K.-P., Eggleton, P. P., & Manners, J. 1997, *MNRAS*, *289*(4), 869.

Raghavan, D., McAlister, H. A., Henry, T. J., et al. 2010, *ApJS*, *190*(1), 1.

Rosas Portilla, F. D., Schröder, K.-P., & Jack, D. 2021, *MNRAS* submitted.

Schmitt, J. H. M. M., Schröder, K.-P., Rauw, G., et al. 2014, *AN*, *335*, 787.

Schröder, K. P., Mittag, M., Flor Torres, L. M., Jack, D., & Snellen, I. 2021, *MNRAS*, *501*(4), 5042.

Schroder, K.-P., Pols, O. R., & Eggleton, P. P. 1997, *MNRAS*, *285*(4), 696.

Tian, H.-J., El-Badry, K., Rix, H.-W., & Gould, A. 2020, *ApJS*, *246*(1), 4.

Tohline, J. E. 2002, *ARA&A*, *40*, 349.

AUTHOR BIOGRAPHY

Dennis Jack is a full professor at the University of Guanajuato. He obtained his Diploma and PhD at the University of Hamburg. In 2012, he moved to Mexico and works on various topics in the field of stellar astrophysics.

SUPPORTING INFORMATION

Additional supporting information may be found online in the Supporting Information section at the end of this article.

APPENDIX A. RV MEASUREMENTS

We present all TIGRE RV measurements of the five binary stars in Table A1.

TABLE A1   Radial velocity (RV) measurements of all stars (also electronically available as Data S1–S6

Stars	JD (days)	RV (km^{-1})
HD 18665	2458366.84840	-5.13 ± 0.12
	2458397.78679	-6.06 ± 0.13
	2458446.74705	-7.98 ± 0.11
	2458466.56093	-8.84 ± 0.14
	2458493.57980	-9.01 ± 0.09
	2458514.57933	-9.27 ± 0.09

TABLE A1   Continued

Stars	JD (days)	RV (km^{-1})
	2458518.57777	-9.12 ± 0.10
	2458692.97971	0.18 ± 0.12
	2458725.83523	5.94 ± 0.11
	2458751.78164	4.30 ± 0.12
	2458771.67443	1.99 ± 0.13
	2458794.69108	-0.22 ± 0.13
	2458814.61678	-2.45 ± 0.11
	2458832.57071	-3.70 ± 0.11
	2458854.58975	-4.45 ± 0.11
	2458875.65306	-5.61 ± 0.11
	2459045.97341	-10.29 ± 0.10
	2459085.84083	-10.10 ± 0.16
	2459118.81388	-9.92 ± 0.11
	2459141.78061	-8.61 ± 0.13
	2459164.72791	-6.88 ± 0.11
	2459195.63323	-1.12 ± 0.11
	2459248.58735	4.88 ± 0.10
HD 27131	2458388.99545	1.72 ± 0.16
	2458446.78764	11.52 ± 0.16
	2458461.73016	16.84 ± 0.13
	2458472.75425	20.49 ± 0.13
	2458491.64267	27.27 ± 0.18
	2458504.65623	31.84 ± 0.08
	2458519.58549	36.51 ± 0.12
	2458539.61070	41.31 ± 0.20
	2458716.98552	18.54 ± 0.14
	2458728.98998	15.85 ± 0.14
	2458743.99337	12.63 ± 0.15
	2458760.84030	9.871 ± 0.17
	2458770.87912	8.19 ± 0.18
	2458784.83426	6.08 ± 0.15
	2458796.76591	4.78 ± 0.26
	2458807.76734	3.55 ± 0.15
	2458817.66481	3.13 ± 0.10
	2458827.65304	2.78 ± 0.15
	2458835.56184	2.95 ± 0.13
	2458845.69483	3.03 ± 0.22
	2458856.64204	4.19 ± 0.13
	2458866.66379	5.39 ± 0.14

TABLE A1 Continued

Stars	JD (days)	RV (km^{-1})
	2458877.58959	6.98 ± 0.11
	2459076.98692	41.53 ± 0.19
	2459120.83843	32.57 ± 0.16
	2459134.81739	29.34 ± 0.20
	2459144.83482	26.94 ± 0.21
	2459158.73090	24.09 ± 0.40
	2459172.77316	20.50 ± 0.26
	2459193.72306	16.02 ± 0.15
	2459204.66835	14.00 ± 0.15
	2459219.65747	11.19 ± 0.16
	2459232.69133	9.22 ± 0.15
	2459255.58633	6.37 ± 0.16
HD 171852	2458250.76875	-22.75 ± 0.15
	2458262.97179	-24.91 ± 0.08
	2458272.87976	-26.44 ± 0.15
	2458276.96559	-27.10 ± 0.13
	2458301.72960	-30.72 ± 0.11
	2458315.79259	-32.69 ± 0.09
	2458324.78002	-34.02 ± 0.11
	2458331.82748	-34.67 ± 0.20
	2458353.67498	-37.83 ± 0.23
	2458385.59252	-40.67 ± 0.17
	2458404.58398	-39.69 ± 0.68
	2458530.02143	-13.22 ± 0.11
	2458547.01505	-14.84 ± 0.10
	2458563.00563	-17.12 ± 0.08
	2458579.97171	-19.61 ± 0.13
	2458598.89813	-23.03 ± 0.16
	2458608.92355	-24.35 ± 0.26
	2458623.78951	-26.71 ± 0.10
	2458638.86077	-29.11 ± 0.11
	2458660.73142	-32.48 ± 0.09
	2458675.74263	-34.35 ± 0.07
	2458695.65868	-36.99 ± 0.09
	2458712.69842	-39.11 ± 0.10
	2458730.65281	-40.59 ± 0.16
	2458748.56696	-41.10 ± 0.12
	2458762.55909	-40.51 ± 0.14
	2458772.56066	-39.37 ± 0.11

TABLE A1 Continued

Stars	JD (days)	RV (km^{-1})
	2458796.55364	-32.04 ± 0.18
	2458898.02129	-15.09 ± 0.08
	2458918.00766	-18.12 ± 0.09
	2458934.00207	-20.71 ± 0.13
	2458949.99080	-23.21 ± 0.09
	2458963.98214	-25.47 ± 0.09
	2458981.97501	-28.24 ± 0.13
	2458995.86851	-30.06 ± 0.12
	2459015.82626	-33.19 ± 0.08
	2459042.75698	-36.83 ± 0.08
	2459076.64807	-40.35 ± 0.11
	2459111.60202	-40.71 ± 0.15
	2459127.56708	-37.77 ± 0.10
	2459145.56472	-32.40 ± 0.13
	2459166.54059	-23.34 ± 0.12
	2459264.02113	-17.68 ± 0.10
	2459293.00521	-22.52 ± 0.13
	2459310.97814	-25.08 ± 0.14
	2459324.98516	-27.43 ± 0.09
HD 215550	2458314.95635	-15.59 ± 0.13
	2458331.81999	-18.02 ± 0.19
	2458349.82508	-18.20 ± 0.15
	2458376.77598	-15.34 ± 0.15
	2458387.69197	-14.30 ± 0.14
	2458401.70564	-13.05 ± 0.10
	2458449.59715	-6.94 ± 0.11
	2458464.61000	-4.96 ± 0.23
	2458476.54501	-3.26 ± 0.11
	2458494.56731	-0.91 ± 0.15
	2458608.95536	14.60 ± 0.14
	2458623.96844	16.01 ± 0.12
	2458648.93751	18.35 ± 0.11
	2458668.91267	17.92 ± 0.10
	2458690.82169	13.50 ± 0.22
	2458707.78405	5.49 ± 0.16
	2458720.76589	-2.28 ± 0.16
	2458730.71462	-7.740 ± 0.10
	2458741.74124	-12.31 ± 0.17
	2458751.63339	-15.47 ± 0.12

TABLE A1 Continued

Stars	JD (days)	RV (km^{-1})
	2458761.66417	-17.14 ± 0.12
	2458770.59163	-17.75 ± 20.10
	2458783.60943	-18.33 ± 0.16
	2458793.58315	-17.69 ± 0.15
	2458813.56829	-16.06 ± 0.10
	2458820.60321	-15.28 ± 0.13
	2458830.56476	-14.13 ± 0.12
	2458841.54270	-12.72 ± 0.09
	2458977.97469	6.09 ± 0.34
	2458987.96966	6.34 ± 0.14
	2458995.96976	7.48 ± 0.14
	2459000.97078	8.31 ± 0.13
	2459012.96938	9.86 ± 0.14
	2459033.94508	12.89 ± 0.17
	2459045.85052	14.16 ± 0.18
	2459076.88206	17.04 ± 0.13
	2459088.75662	18.01 ± 0.17
	2459106.71727	17.76 ± 0.14
	2459117.69385	16.33 ± 0.16
	2459127.67240	13.46 ± 0.31
	2459141.61819	6.90 ± 0.10
	2459151.60453	1.29 ± 0.11
	2459162.60925	-5.34 ± 0.14
	2459172.57873	-10.13 ± 0.25
	2459182.54953	-14.22 ± 0.11
	2459195.54626	-16.99 ± 0.14
	2459208.57139	-18.02 ± 0.14
	2459328.98114	-6.53 ± 0.21
HD 217427	2458314.95475	-22.47 ± 0.09
	2458331.82149	-23.76 ± 0.20
	2458351.80596	-24.99 ± 0.11
	2458385.71645	-26.54 ± 0.13
	2458449.59554	-31.40 ± 0.10
	2458497.56869	-34.76 ± 0.17
	2458631.95965	-17.23 ± 0.10
	2458650.96811	-17.92 ± 0.09
	2458670.91219	-19.14 ± 0.10
	2458693.83997	-20.47 ± 0.08
	2458708.79431	-21.30 ± 0.10

TABLE A1 Continued

Stars	JD (days)	RV (km^{-1})
	2458724.82595	-21.70 ± 0.08
	2458739.74297	-22.73 ± 0.13
	2458753.70438	-23.58 ± 0.12
	2458768.63801	-24.27 ± 0.14
	2458783.64526	-25.37 ± 0.11
	2458798.61809	-26.79 ± 0.11
	2458813.56671	-27.79 ± 0.08
	2458827.58366	-28.90 ± 0.09
	2458842.55102	-29.62 ± 0.12
	2458979.97344	-22.22 ± 0.12
	2458994.96788	-18.71 ± 0.12
	2459003.97033	-17.45 ± 0.10
	2459019.96992	-16.74 ± 0.11
	2459040.97416	-16.93 ± 0.10
	2459076.84217	-18.42 ± 0.11
	2459095.72271	-19.44 ± 0.15
	2459116.71672	-20.19 ± 0.16
	2459132.69030	-21.29 ± 0.13
	2459146.57782	-22.20 ± 0.11
	2459162.61127	-23.52 ± 0.08
	2459177.54677	-24.51 ± 0.12
	2459198.54290	-25.78 ± 0.11